Fall 2020

Mid-infrared chiral metsurface coupling with molecular vibration

Md Shamim Mahmud

Department:

MID-INFRARED CHIRAL METASURFACE COUPLING WITH MOLECULAR VIBRATION

by

MD SHAMIM MAHMUD

A THESIS

Presented to the Graduate Faculty of the

MISSOURI UNIVERSITY OF SCIENCE AND TECHNOLOGY

In Partial Fulfillment of the Requirements for the Degree

MASTER OF SCIENCE IN MECHANICAL ENGINEERING

2020

Approved by:

Dr. Xiaodong Yang, Advisor
Dr. Jie Gao
Dr. Cheng Wang

ABSTRACT

The mid-infrared design of chiral metamaterial shows a tremendous absorption capability of infrared rays, and it has the significant application of circular dichroism based device development. Plasmon-phonon coupling is one of the application of metamaterial that provides a new path for tailoring the surface in the nanoscale, which is also applicable in molecules detection. It is possible to change the Plasmon-Phonon coupling strength not only through the chemical change of molecules but also by changing the metamaterial light-matter interaction property. So far, linearly polarized light shows the strong coupling between metamaterial and molecules. However, it is possible to observe strong coupling in circularly polarized light by fabricating the chiral metasurface. In this research, we introduce two types of new chiral metasurface that has strong interaction with the molecules in different circular polarization of light, which exhibits over 58% and 65% circular dichroism (CD) in the mid-infrared region (5- 6 μm). By adjusting the geometric parameters of the new chiral structure of single-sized unit cells, it is possible to shift the absorption peak in the various midinfrared range. Besides that, we design the broadband resonator by combining the multiple chiral structures. For the molecule's detection, It also shows a higher splitting gap in the right circularly polarized light in compare to Left circular polarized light. Our numerical and experimental result of the C=0 bands signals which emits from polymethyl methacrylate (PMMA) film using chiral metasurface unveils the effective way for tuning the coupling strength of molecules in circular polarization of light.

ACKNOWLEDGMENTS

I would like to extend my sincere appreciation to Dr. Xiaodong Yang for being my advisor and for all his constant support, guidance, and expertise during my graduate study at Missouri University of Science and Technology and especially for his help with the preparation of this thesis. I also want to thank my other committee members, Dr. Jie Gao and Dr. Cheng Wang, for their valuable time and for supporting me for my research progress.

Furthermore, I am grateful that I got many opportunities under Dr. Yang's supervision in the nanoscale optics lab. Dr. Yang provided Graduate Research Assistantship and Teaching Assistantship as financial support, which helped me to continue my research. Lastly, I would like to express my love to my family and my friends for their inspiration during the master’s program.

TABLE OF CONTENTS

Page

LIST OF ILLUSTRATIONS

Page

LIST OF TABLES

Page

NOMENCLATURE

Symbol	Description
A_+	High absorption
A_-	Low absorption
P	Periodicity
δ	Splitting gap
ρ	Material density
C_p	Heat capacity
K	Thermal conductivity

1. INTRODUCTION

1.1. METAMATERIAL

Electromagnetic (EM), metamaterials (MMs), metasurfaces (MSc) all are the rising field and it has tremendous application in sensor development which plays an important role in 21st century device development. Metasurface is the surface that changes the material property artificially. It is composed with a subwavelength metal/dielectric structure that usually creates the coupling mode with the incident electromagnetic wave, which exhibits a property that's not found in nature: extensive loss and material dispersion associated with the metallic and dielectric compound structure. So, the appropriate material choice is one of the critical factors to get a good result based on the desired application field. Phase gradient one of the main characteristics that is followed by the conventional optical components during the propagation of light inside the two different medians. Multiple degrees of freedom which consists multi-dimensional array of optical resonators (based on their size and position) could introduce multiple directional phase change in the same medium. Using Electromagnetic metamaterials (MMs) and metasurfaces (MSs) it is not only possible to localize electromagnetic filed, but also decode and analyze the signal of the incident light. Hence, introducing the resonant mode in the metastructure by boosting the interaction between the analyte layer is widespread interest in sensing platform development. In this research, we will discuss the possible application of metasurface structure for molecules detection where the absorption energy depends on the subwavelength metallic structures shape, position, and

presence of a dielectric medium. Based on this absorption capacity, the molecular detection sensor is usually fabricated.

1.1.1. Chirality. Chirality is the universal property of matter that frequently found in nature. Chiral material represents two enantiomeric forms that cannot be superimposed (Figure 1.1) with each other by changing is orientation or position. In a chemical perspective chiral compound obtained in two different forms where molecular structure are identical but different combination could be found in multi-dimensional arrangement of atoms such that they are no superimposable in the mirror reflection. For example, the two enantiomeric forms of amino acid are:

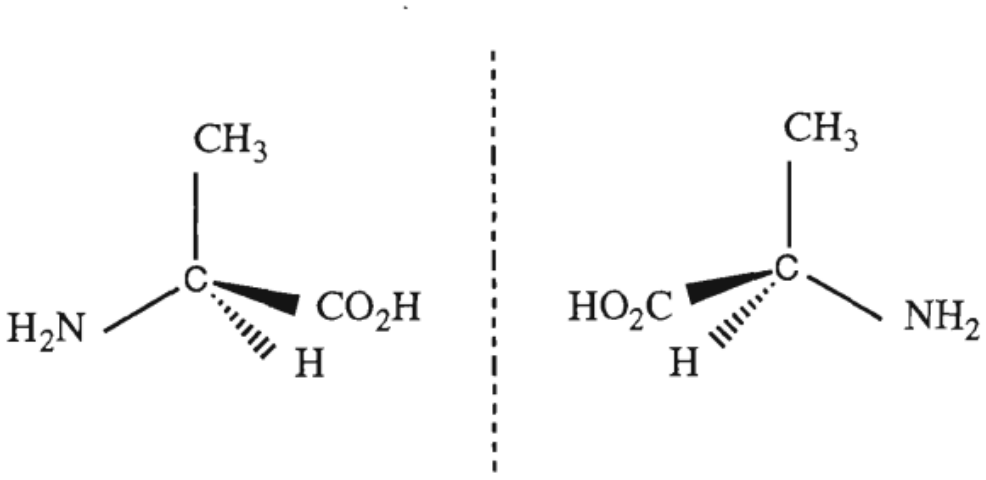

(-) alanine (+) alanine

Figure 1.1 Chiral molecules.

The chiroptical response, especially the circular dichroism (CD) and electromagnetic behavior, can see in various organic materials like amino acid. It has a significant impact on left and right circularly polarized light, such as (LCP) and (RCP) mode. One of the examples is Faradays isolators that are built upon on the faraday effect, which induced by an external magnetic field. Although, the material which found in nature the chiral response is very week in engineering application. However, fabricating the metamaterial in asymmetric structural format can solve this issue, which shows the strong chiroptical response. Usually, metamaterial composed of subwavelength metal/dielectric structure which couple with the electric or magnetic components due to the incident of electromagnetic wave and exhibits a property that's not available in nature. The combination of chirality and metamaterial property can apply in sensor development [1, 2]

1.1.2. Sensor. Raman scattering is one of the methods where an inelastic scattering of photon excited to higher energy levels. The scattered light is used for material detection and analysis. However, a small fraction of photons are scattered by laser excitation, so there for a small percentage of probability of Raman scattering. The beginning of the 21st-century researcher has been using gold or silver as a plasmonic metal for developing a nanostructure-based sensor, which is called a surface plasmonic sensor. In the case of using a plasmonic metasurface structure for sensor applications, we need to focus on a high electron cloud-based metal surface. When choosing a material, it is usually best to pick the one with the least amount of ohmic loss, and therefore the lowest dampening rate. The energy transportation mechanism of the atom inside the metamaterial plays a vital role in introducing absorption and transmission phenomena.

The atomic vibration takes place on the top of the metal surface caused by the absorption of electromagnetic energy. After absorbing the energy, the atom starts to vibrate from its position and reemit the absorbing energy as a new wave in the same frequency as the first wave was. During this propagation, the secondary molecular vibrations occur for only a short period. As a result, the motion of the wave gets slower when it passes through the medium. The space between the two atoms works as an energy transfer passage when once an atom reemits the energy of the electromagnetic wave. Once the energy emitted from the first atom, the next atom absorbed the transmitted energy and generate electron vibrations and then again reemitted energy into the next atom. In between the emission and absorption process, some time delay takes place. The speed of the electromagnetic wave same as the speed of light: c (3×10^8 m/s) through the vacuum of interatomic space. During this traveling, the net traveling speed hindered for re-emission and absorption process, that is why the actual speed of the EM wave should be less than c. Additionally, the optical density of the material also defines the actual speed of an electromagnetic wave through a material. Material property changes the delay time during the absorption and remission process. Furthermore, the packing factor plays a vital role in whether the material atoms are tightly packed or not. If the packing factor is too high, then the amount of distance between atoms is less. Depending on the nature of the material, the packing factor impacts the electromagnetic wave propagation length. When the electromagnetic wave propagates on the metal surface under a resonant condition, due to the plasmonic effect, two situational could appear: Localized surface plasmon resonance (LSPR), surface plasmon resonance (SPR). If the evanescent field in the dielectric medium is shorter than the surface plasmon propagation length, than that is called the localized

surface plasmon resonance. To create the LSPR, we take the adaptive optics technique (Figure 1.2) where the incident electromagnetic wave faces match with the electromagnetic transmission wave inside the metal. Hence the different size of the nanostructure is fabricated on the top of the surface for localizing the surface plasmon resonance. There is some limitation in the case of using plasmon resonance for sensor application. Every vibration follows the specific frequency for the incident electromagnetic wave. Any material has various resonance frequencies based on the atomic level but has only one plasma material working as a reflector.

$$\varepsilon_r(\omega) = 1 + \frac{\omega_p^2}{\omega_0^2 - \omega^2 - i\omega\gamma_o}$$

Plasma frequency:

$$\omega_p^2 = \frac{Nq^2}{\varepsilon_r m_\varepsilon}$$

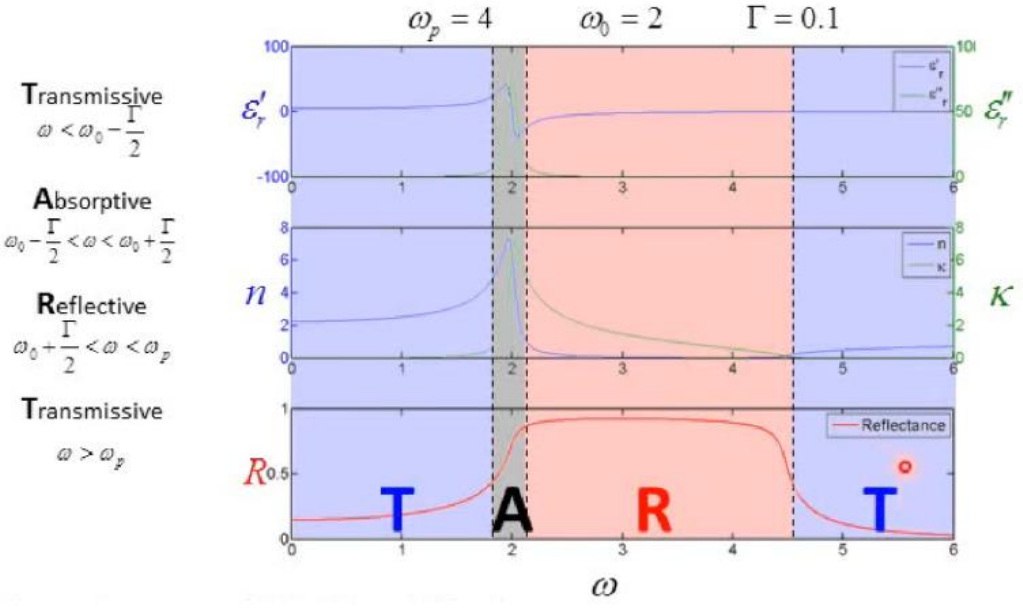

Figure 1.2 High absorption in resonance frequency.

2. CHIRAL METASURFACE ABSORBER

2.1. BACKGROUND

The metamaterial is the artificial material that exhibits a property that does not find in nature. This artificial property of metamaterial is applicable in various optical device development. One of the significant applications is metamaterial-based thermal emitter [3-5]. Additionally, it can be used in the thermal imaging system, low-cost gas sensing, and Shockley –Queisser limit [6-8]. In recent times, metamaterial with chiral property draws considerable attention in the research community. The left-circularly polarized (LCP) and right-circularly polarized (RCP) light-matter interaction introduced new property and application of metamaterial. Kirchhoff's law tells that the emissivity of a material proportional to the absorptivity. So we can predict the thermal emissivity of a metamaterial-based on light absorptivity. As a result, gases like CO_2 characteristic line in the near-IR region while the absorption in longer wavelength is strong. Most of the Thermophotovolatics (TPV) system with high bad-bandgap semiconductor research on the resonant frequency of 1.75 μm [9] where thermally stable and high electromagnetic absorption materials like Ti, W, Al_2O_3 are usually used [10-12]. Hence, the combination of the chirality and metamaterial property that can be applied as a polarized light absorber in addition to mid-infrared TPV system development would be a great endeavor.

Usually, chirality is the universal property of matter that frequently found in nature and material, which found in nature the chiral response is very week in engineering application. For solving this issue, the researcher uses the top-down or bottom-up process to design the chiral metamaterial for device development. The recent

progress of chiral metamaterial design revels much more complicated structures such as L-shaped, twisted crosses [13, 14], spirals [15-17], and entangled structures [18, 19]. But the use of those metamaterial varied case by case due to the nature of the application, such as all-metallic, metal-dielectric, all-dielectric metamaterial absorber. All metallic light absorber used as a light absorber, while metal-dielectric metamaterial is most appropriately applicable for thermal emitter [20, 21]. The combination of metamaterial design and thin layer gives the optimal thermal absorptivity. Since geometrical design dominates the resonance mode of a single resonator, there are several methods available to obtain broadband absorption. The present study shows that the use of metal-insulator-metal chiral structure absent from the development of mid-infrared chiral thermal emitter. Previously the metamaterial is used as a thermal absorber for linearly polarized light [22]. Additionally, the design is very simple, and the chiral property is shown. To address this gap of research, we designed a new chiral metamaterial that can absorb mid-infrared in LCP light condition and also indicates the low absorption rate in the RCP light condition. Our designed chiral metamaterial shows the high efficiency in the near-infrared region, and the high absorption CD is observed due to the unique pattern of the metallic layer. It is possible to maximize the absorption CD by sweeping the geometric parameter of our designed structure. For a better understanding of the mechanism of chiral optical absorption, electric field distribution is explained for the LCP and RCP condition of the incident light. Finally, we have included the thermal analysis as a potential application in the mid-infrared range for metamaterial absorbers. We also demonstrated the implementation of our newly designed device for the broadband absorber application.

The result also provides the new opportunity to develop an optical filter, an optical communication device, and chiral imaging [23-25].

2.2. CHIRAL ABSORBER DESIGN

We design the unit cell of a periodic coplanar chiral metamaterial shown in Figure 2.1(a). The Au-Al_2O_3-Au three-layer is grown by an electron beam evaporation method on a silicon substrate.

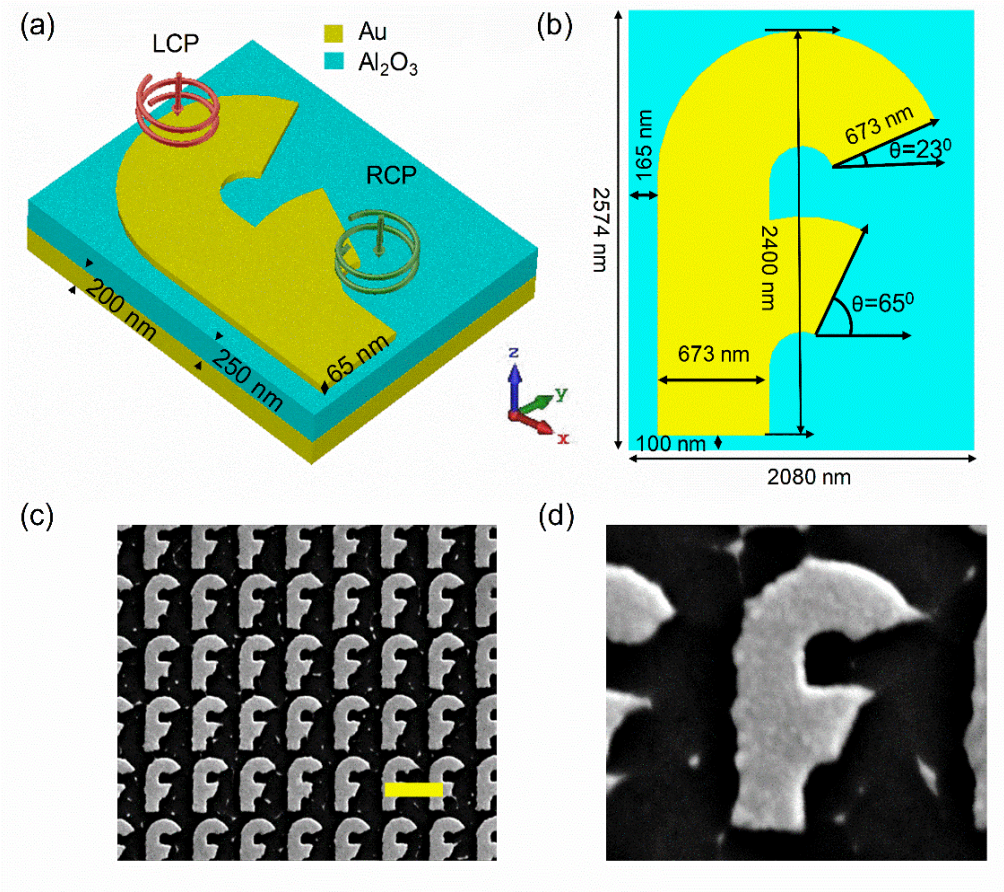

Figure 2.1 Chiral metasurface designed on a Au layer. (a) Structure of the designed plasmonic metasurface and the incident light configuration. (b) Unit cell period p_x=2.08 μm, p_y=2.57 μm (c) FIB fabricated nanostructure on a silicon substrate. Yellow Scale bar: 2 μm. (d) Single unit cell.

Argon (*Ar*), atmosphere 5 mTorr pressure with a flow rate of 0.08 A_0/Sec, is used to grow Al_20_3. We deposit the gold film onto the alumina layer with an evaporation flowrate 0.5 A_0/Sec. The nanostructures are fabricated in the gold film using the top-down process of the Focused Ion beam system (FEI Helios Nanolab 600, 30 kV, 28 pA). The resonator design looks like the shape of "F" where the periodicity P_x (2.08 μm), P_y (2.57 μm) in *x* and *y* direction subsequently. The design is inherent of two gold (*Au*) layers of thickness, 65 nm for the upper layer, and 200 nm for a bottom layer, which is separated by an alumina (Al_2O_3) layer of thickness 250 nm. The asymmetrical design of the chiroptical structure resonance response mechanism depends on the curvature of its arm. The asymmetric cut-out in *x* and *y* direction formed the chiral structure on the top of the alumina layer. Figure 2.1(c) describes the diagram and scanning electron microscopic (SEM) image of the 2D-chiral metasurface, which is manufactured by a focused ion beam on the top of the 65 nm thickness of the gold layer.

2.3. RESULT AND DISCUSSION

The FTIR signal shows the 2D-chiral response from the metamaterial. For measuring the absorption spectra and CD, achromatic twenty-four plate (eo Edmund optics) in addition to linear polarizer is used to convert FTIR (Thermo Scientific, Nicolet 4700) tungsten halogen source to produce circularly polarized waves. Then 20X objective lens is used to focus the resulted light source onto the sample using a. Another 20X objective lens is used flowing by previous on to collect the reflected light, which then directed to a spectrometer (Horiba, iHR 550). As a reference for normalizing the reflected spectra, a silver-coated mirror (THORLABS) is used. The metamaterial designed consists

of asymmetric configuration in x and y direction while the z-direction is symmetric. The experiment also reveals that the electromagnetic field confinement (Figure 2.1(d)) of an asymmetric surface depends on the curvature of the structure.

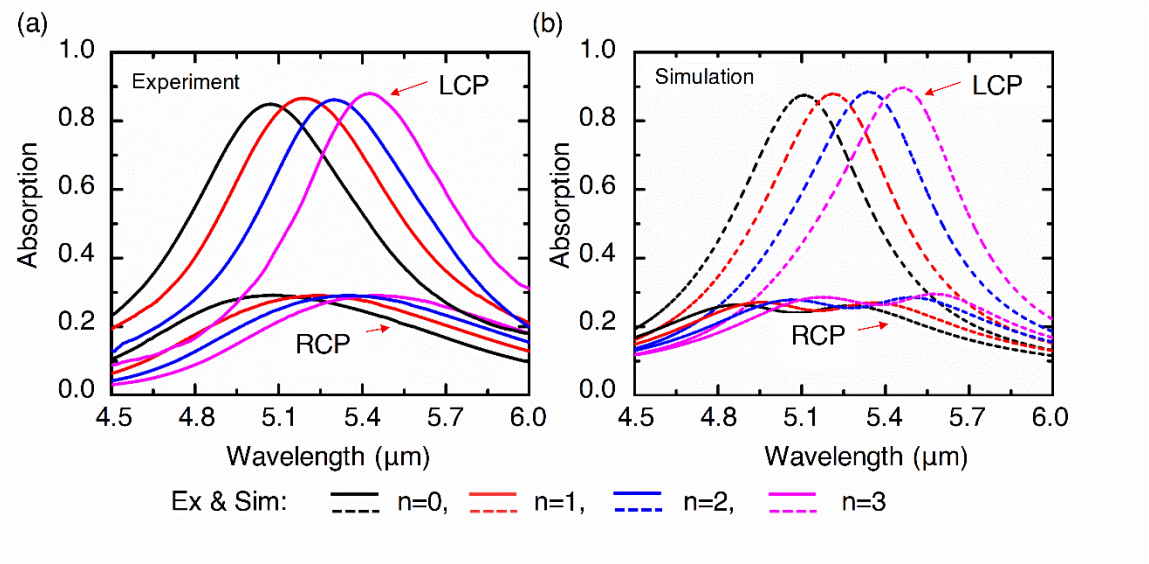

Figure 2.2 Spectra measurement in different periodicity ($p*k^n$): where, p = (p_x = 2.57 μm, p_y =2.08 μm) k = 1.02 and n = 0, 1, 2, 3 (a) FTIR measured absorption spectra (b) Simulated absorption spectra.

Due to the concentration of the EM field in the curve of the structure, it helps to produce the single-pole mode, which contributes to the circular dichroism (CD). Additionally, we apply the genetics algorithm for structural optimization to obtain higher CD values from the EM field concentration. The $\theta = 23^0$ rotation of upper curvature and 65^0 rotation of lower curve shows the optimum structural condition, and the structure maximizes the chiral response with a CD of 0.58 in the 5.11 μm wavelength. The FTIR measurement spectra show that the absorption capacity in the RCP approximately 26% and ~84% for LCP. The CD calculation has been done based on the equation, $CD =$

$(|A_+ - A_-|)\%$, where $A_\pm$ are absorbances for the RCP and LCP incident wave which are given by $A_\pm = 1 - R_\pm - T_\pm$. As it is the three-layer of structure, so we assume that the $T_\pm = 0$. Figure 2.2 points out the effect of periodicity (p) change by maintaining the scaling factor n. For obtaining an absorption peak in the desired frequency region, we formulated the scaling factor n with a function of periodicity p and constant k, which constitute as $p*k^n$. The simulation and experimental results show the smooth transition of LCP and RCP peak with the change of n value in a wide range of spectra.

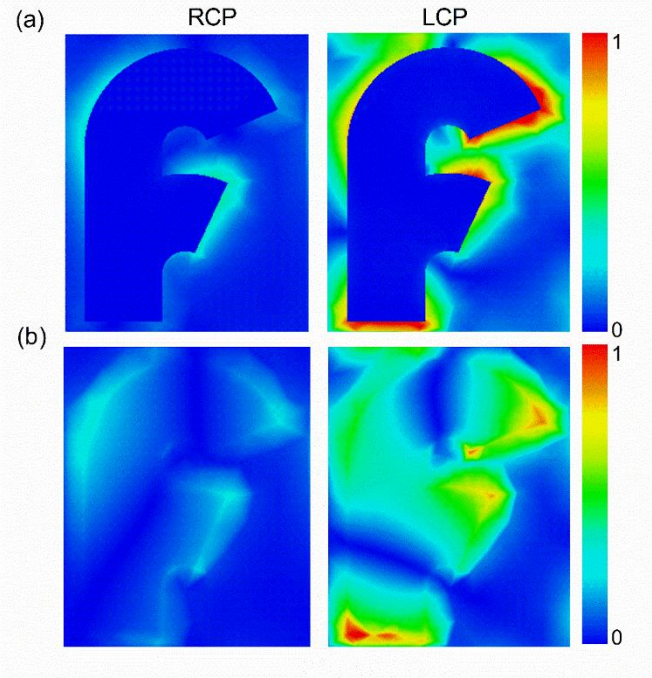

Figure 2.3 Simulated field of "F" structure. (a) Electromagnetic field distribution on the gold surface (b) LCP, RCP mode in 5.11 μm wavelength which is located 10 nm underneath of the gold layer.

In this simulation, the permittivity of the gold is taken from Rakic et al. 1998: Brendel-Bormann model [26] and Alumina from Kischkat et al. .2012 [27]. All simulation has been done

in using CST frequency Domain Solver. For the boundary condition, the unit cell option is used in the X and Y direction. The Z-direction was open to allow the incident of a vertically plane wave on the periodic structure. For the resonant condition, the Drude model is used to assume the permittivity of the bulk gold in the mid-infrared, $\varepsilon_{Au} = \varepsilon_{\infty} + \frac{\omega_p^2}{\omega^2 - i\omega\gamma_o}$, where the background dielectric constant is $\varepsilon_{\infty} = 1$, the plasma frequency $\omega_P = 1.37 \times 10^{16}\ rad/s$ rad/s and the damping constant $\gamma_p = 4.08 \times 10^{13}\ rad/s$. We simulated the absorption, electric field and temperature distribution of designed metamaterial based on different polarization to determine the underline mechanisom. Figure 2.3 plots the simulated electrc field $|E(r)|$ for the structure of n=0, which shows the maximum electric field concentration take place at the edge of curve surface. Both the top surface and inside the space layer the plasmonic resonance enhanced in the incident of LCP light rather than the RCP light.

Furthermore, we solve the heat transfer equation to investigate the temperature distribution $\nabla.(k\nabla T) = q$, where temperature, thermal conductivity, and heat generation density in metal is defined by *T*, *k* and *q* subsequently: $q(r) = \left(\frac{\omega}{2}\right) Im[\ \varepsilon(\omega)]\varepsilon_0|E(r)|$. In this thermal simulation, we consider the incident light onto one unit cell around 10 μW, corresponding to 30 μW/m^2. The assumed boundary condition is periodic around the unit cell where the top is open. The top and bottom temperatures are fixed around 300 ^{0}C, where the heat is mostly generated on the top gold layer. Table 2.1 describes the thermal parameters which have been used in this research. For the COMSOL simulation purpose, we consider the 100 μm *Si* substrate as a bottom layer of the device. The strong absorption of the LCP light triggers the increase of electromagnetic concentration in the metallic gold layer, which farther leads to generate more thermal energy where in comparison to LCP, the thermal generation RCP is low.

The top layer, which is built by gold material, achieves the higher temperature distribution in contrast to surroundings due to its higher thermal conductivity in where inside the "F" structure, the heat remains constant. The thermal circular dichroism (CD_T) for our experiment is 20 K, where the temperature for the LCP and RCP cases are 335.2 K and 315.2 K subsequently.

Table 2.1 Thermal properties of the material for heat transfer analysis.

	ρ (kg m^{-3})	**C_p (J kg^{-1}K^{-1})**	**k (W m^{-1}K^{-1})**
Gold	19320	129	315
Alumina	3970	765	1.6
Silicon	2330	712	148
Air	1	353[K]/T	0.03

We focus on the periodic structure of the metasurface to estimate the thermal distribution. Usually, in the resonance mode, thermal absorbance is too high, where Figure 2.4(a) shows the thermal distribution on the top of the gold layer. We see the uniform thermal distribution around the "F" structure in all directions (Figure 2.4(c)). In the steady-state heat transfer, thin-film thermal conductivity decreases dramatically at the nanoscale because of the interfacial scattering effect. In metamaterial between two anisotropic surfaces, the thermal distribution impedes due to the obstruction of

vibrational energy transfer. It assumed that the surface and the bulk material heat capacity is the same. For the structure of n=0 and the wavelength of 5.11 μm, the structure shows its resonant condition, which evolves as a thermal output.

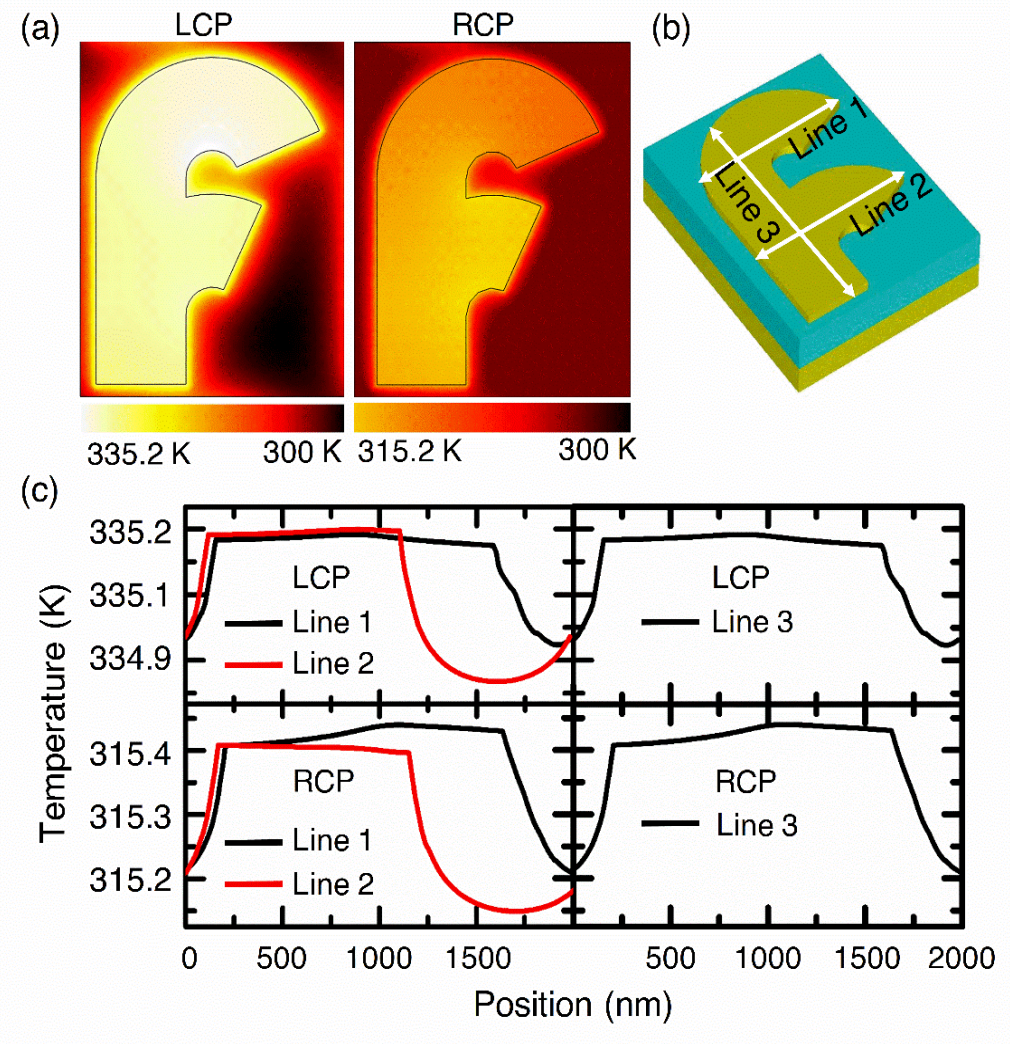

Figure 2.4 Heat generation on "F" structure. (a) Thermal distribution on the gold layer for the wavelength of 5.11 μm (b) Temperature distribution line (c) Temperature distribution along the line under polarized mode.

In our designed structure, we observe that not only periodic structure helps to shift the absorption pick but also the angle of curvature allows the shifting of resonant pick in

different wavelengths. Hence by fixing the upper curve 23^0 (Figure 2.5(a)), if we change the lower curve angle from 65^0 to 0^0, then the absorption pick will be shifted from left to right direction that indicates the resonant wavelength increases. If we increase the edge 65^0 to 130^0, then the pick will change in the left path, and the resonant wavelength decreases. As a result, it is possible to find the broadband absorption pick in the mid-infrared range in our optimized structure. So, we design the broadband meta-structure based on 23^0 and 65^0 curvature angle by only changing the periodic (n) parameter.

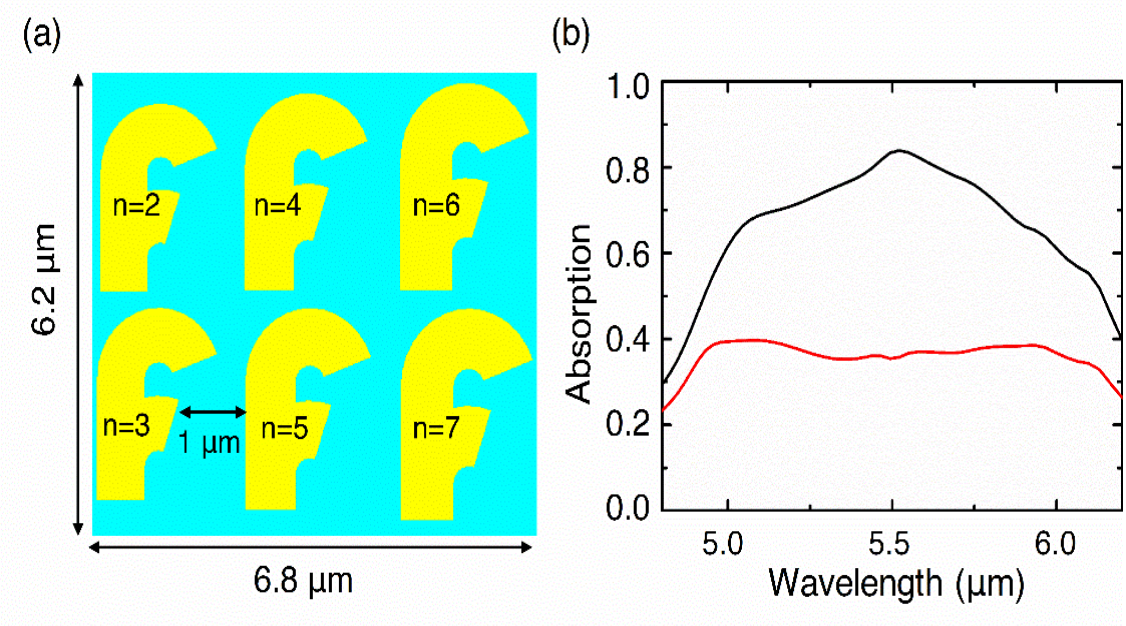

Figure 2.5 Broadband design. (a) Distribution of " F " structure pattern in multiple design size. (b) Broadband simulation.

We calculate the numerous design combination of n parameters to obtain the flatten and broaden circular dichroism in the range of 5 µm to 6 µm. Our optimum 'n" parameter combination is shown in Figure 2.5(a) while Figure 2.5(b) is the corresponding output of absorption spectra. In this broadband absorption experiment, we get the highest

absorption pick in the middle of the broadband range for the LCP light incident is 0.82, and the lowest absorption pick for RCP light incident is 0.38. Hence our maximum CD is around 0.44 for the broadband absorption spectra. The RCP spectra are much straighter than the RCP spectra. It happens due to the interaction of electric field concentration around the periodic structure. If we carefully observe the Figure 2.3 we may see that the unit cell EM concentration is higher in the bottom of “F ” structure as well as the edge of curvature in LCP cases. This bottom and edge concentration of the EM field is profoundly affected by the surrounding structure. So when we put the different size (n) of the periodic structure, it mostly hindered for flattening LCP curve. In contrast, the RCP curve remains flattered due to the lack of surroundings structural effect.

3. 2-D CHIRAL SELECTIVE SURFACE

3.1. BACKGROUND

Previously metamaterial property used in biochemical sensor development [28-30], surface-enhanced spectroscopy [31, 32] negative refractive index [33, 34] nonlinear optics [35, 36] invisible cloaking [31, 37], and quantum computing [38]. In the biochemical sensor application, metamaterial suppresses the transmission and reflection while the energy dissipates in the absorbing layer. Due to the absorption of energy, the nanostructure response appears as localized surface plasmonic(LSP) and surface plasmon polariton (SPP) [39, 40]. When the molecules deposit on the metasurface for sensing purpose then the coupling phenomena takes place between the molecular vibration (phonon) and plasmonic metasurface, especially when the plasmon energy transition is in resonance with electromagnetics mode. The coupling strength between the molecules and metasurface associate with the metasurface design and the absorption capability of that multilayer structure. As well as the stronger coupling strength found when the rate of coherent exchange of energy between light and multilayer structure is higher than their decay rates [41, 42]. Several researchers have shown strong coupling experimentally, where they able to confine the electromagnetic field into nanostructure using metallic optical cavities [43, 44].This delicately fabricated metallic structure produces collective excitation of periodic nanostructures which could be used as a molecular sensing platform [45, 46] or local resonance of single metal molecules. Both types of structures are good because the enhanced EM field can provide a vibrational fingerprint of molecules. As well as infrared (IR), fingerprint vibration contains valuable molecular

information that directly linked to molecular property and chemical bonds. It is found that the two plasmonic modes of the metasurface, which couple with two vibrational modes of PMMA molecules, can provide more reliable sensing information [46-48] where metasurface design plays an important role in detecting vibration fingerprint of biomolecules. However, the research on chiral metasurface with a circularly polarized infrared ray is still missing from the study on strong plasmon phonon coupling for molecules detection. For the metamaterial, a planar chiral multilayer resonant structure in the shape of gammadion designed in the near-infrared regime where strong circular dichroism (CD) observe with a value of 50%. Recently chiral selective silver plasmonic η shape metasurface absorber is developed in the visible frequency [49]. The research shows that the LCP and RCP values are getting high at a different frequency level. Additionally, the dielectric medium and metal layer of metamaterial affect the CD property. Vanadium dioxide(VO_2) [24, 50] based negative structured metasurface shows a significant high LCP and RCP where the polarization rotation is almost 20 degrees in Terahertz wavelength. Mashiko Shioi developed a gold-based (AU $-SiO_2-$AU) positive structure where localized surface plasmons can control dependent on the array period and diameter of the metasurface33. Fei Cheng explained a plasmonic-enhanced biosensing device for a gold-based negative structure. However, it is still missing the chiral effect of structure and the high CD value, although the air gap of the negative structure is more than 100 microns. All those research shows the metasurface design importance for controlling the plasmon effect; however, no significant LCP and RCP property were shown for controlling the molecule's detection level.

3.2. CHIRAL DESIGN

We design chiral metamaterial with a periodic structure, which is shown in Figure 3.1(a). The unit cell arranges in the shape of the "eye" with the period of Px (1.8 μm), Py (2.1 μm) in X and Y direction subsequently. It consists of two gold (Au) layers of thickness, 65 nm for the upper layer, and 200 nm for a bottom layer, which is separated by an alumina (Al_2O_3) layer of thickness 250 nm. The asymmetric elliptical cut-out section in X and Y direction inside each unit cell connected in a vertical direction. Figure 3.1(c) describes the structure of the metamaterial and scanning electron microscopic (SEM) image of the 2D-chiral metasurface, which is fabricated by a focused ion beam (FIB) on the top of the 65 nm thickness of the gold layer.

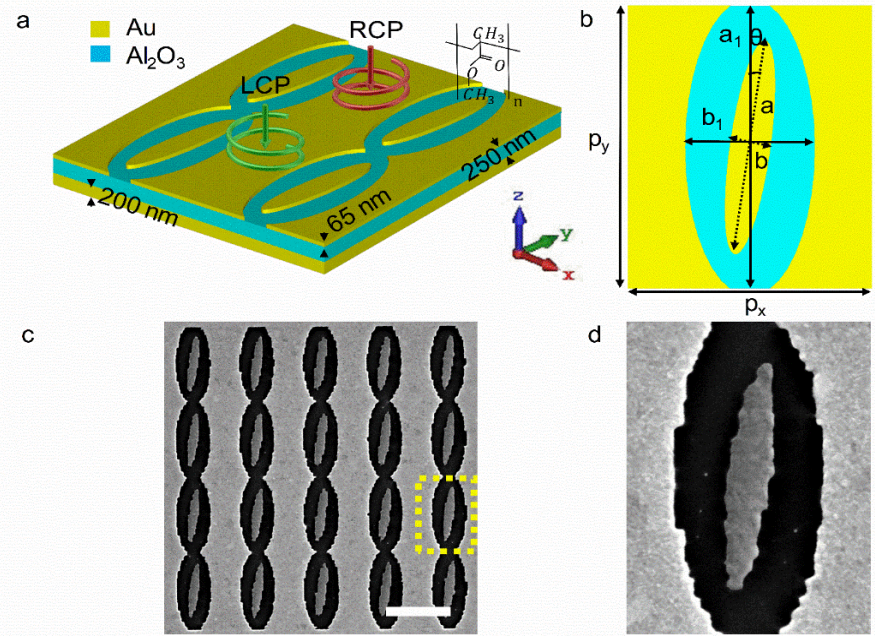

Figure 3.1 Chiral metasurface fabricated on gold film. (a) Structure of the designed mid-infrared metmaterial and polarization configuration. (b) Metamaterial period p_x=1.8 μm , p_y=2.1 μm; outer elliptical shape a1 = 2.2 μm, b1 = 1.0 μm; Inner elliptical shape a = 1.6 μm, b = 0.3 μm; rotation angle θ=80. (c & d) Selected nanostructure SEM image. Scale bar: 2 μm.

3.3. METHOD

Our experimental process is segregated in multiple steps. We repeated the whole process several times to optimize the experimental result. Finally, we try to match the experimental result with simulation result.

3.3.1. Sample Fabrication. The Au-Al2O3-Au three-layer is grown by an electron beam evaporation method on a silicon substrate. Argon (Ar), atmosphere 5 mTorr pressure with a flow rate of 0.08 A0/Sec, is used to grow Al203. We deposit the gold film onto the alumina layer with an evaporation flowrate 0.5 A0/Sec. The nanostructures are fabricated in the gold film using the top-down process of the Focused Ion beam system (FEI Helios Nanolab 600, 30 kV, 28 pA).

3.3.2. PMMA Layer Preparation. Different thickness of poly (methyl methacrylate) is used in this experiment. The thin layer of PMMA (950-A2, MicroChem) is deposited through the spin coating on the top of the metamaterial. For varying the PMMA layer thickness, 2000 rpm and 3000 rpm is used in multiple time. The X-reflection result shows that the 2000 rpm and 3000 rpm of spin coating gives 80 nm and 60 nm thickness of the PMMA layer. So, for getting 140 nm thickness of the PMMA layer, we first use 2000 rpm and top of that layer, we use 3000 rpm deposition. Hence the total thickness reaches approximately 140 nm, which is verified by FIB cross-section measurement. Similarly, 200 nm deposition is done by using 2000 rpm, 3000 rpm, and 3000 rpm subsequently.

3.3.3. Optical Characterization. For measuring the absorption spectra and CD, achromatic twenty-four plate (eo Edmund optics) in addition to linear polarizer is used to convert FTIR (Thermo Scientific, Nicolet 4700) tungsten halogen source to produce

circularly polarized waves. Then 20X objective lens is used to focus the resulted light source onto the sample using a. Another 20X objective lens is used flowing by previous on to collect the reflected light, which then directed to a spectrometer (Horiba, iHR 550). As a reference for normalizing the reflected spectra, a silver-coated mirror (THORLABS) is used.

3.4. ANALYSIS OF COUPLING BEHAVIOUR

The FTIR signal shows the 2D-chiral response from the metamaterial. The metamaterial designed consists of asymmetric configuration in X and Y direction while the Z direction is symmetric. The experiment also reveals that the electromagnetic field confinement of asymmetric surface depends on the rotation and dimension of an inner positive elliptical structure corresponding to the outer negative elliptical structure. Hence, we apply the Trust Region Framework algorithm for structural optimization to obtain maximum circular dichroism (CD). The $\theta=8^0$ rotation of positive elliptical structure with a base dimension of a =1.6 μm and b= 0.3 μm while the outer negative elliptical shape dimension a1, b1 is 2.2 μm and 1.0 μm represent the optimum structural configuration. If we multiply the periodicity p (p_x, p_y, a, b, a1, b1) with a constant k (1.05) in the order of $p*k^1$, then it shows the maximum CD in the frequency of 57 THz. In the above optimum structural condition, the structure maximizes the chiral response with a CD of 62.5%. In the FTIR measurement, spectra revel 91% absorption capacity RCP and 21% for LCP. For the calculation of the CD, the fitness to be maximized is defined as,

$f = |A_+ - A_-| = |T_+ - T_-|, CD = \left(\frac{|A_+ - A_-|}{|A_+ + A_-|}\right)$ %, where $A_\pm$ are absorbances for the RCP and LCP incident wave which are given by $A_\pm = 1 - R_\pm - T_\pm$. As it is the three-

layer of structure, so we assume that the $T_{\pm}$=0. Figure 3.2 represents the change of period (p), which maintains the specific aspect ratio. For obtaining absorption pick in the desired frequency region, we multiply the period p with a constant k, k^1, k^2 k^3 k^4, $k^{5,}$ and It shows the smooth transition of LCP and RCP pick with the change of periodicity in a wide range of spectra, which is pretty much matches with the experimental result.

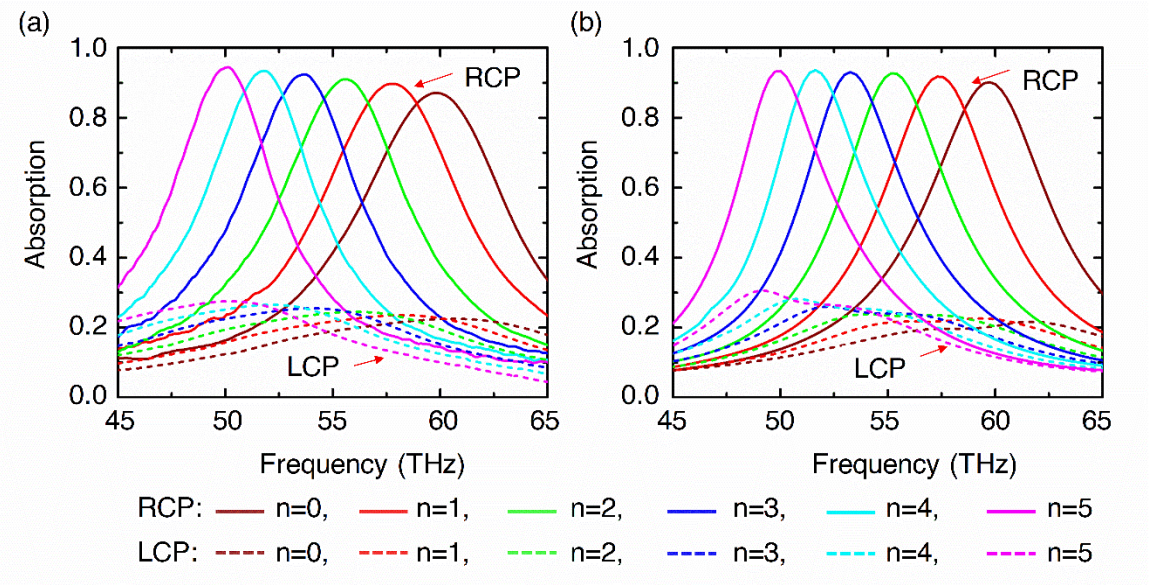

Figure 3.2 Spectra measurement in different periodicity: p (px=2.1 µm, py=1.8 µm, a1=2.2 µm, b1=1.0 µm, a=1.6 µm, b= 0.3 µm), k=1.05 (a) FTIR measured absorption spectra b) Simulated absorption spectra.

Usually, PMMA molecules, especially C=0 bond excites in the mid-infrared frequency of 52 THz. We apply the PMMA molecules on the top of the optimized metasurface structure, which has a dimension p*k^1 and high CD in 57 THz frequency. Without taking the coupling condition, the simulation result shows the shifting of LCP-RCP pick from 57 THz to 52 THz where the PMMA permittivity is assumed to be constant ($\varepsilon_{PMMA} = 2.2$). Now applying the Lorentz oscillator model in PMMA spectra,

we get the plasmon phonon coupling in the frequency of 52 THz (Figure 3.3). Here we take the three different thicknesses (80 nm, 140 nm, 200 nm) of PMMA to see the coupling strength. The strong coupling between localized surface plasmon (LSP) and the phonon open the two-absorption maximum in RCP mode and two absorption minimum in the LCP mode. This splitting behavior represents the coupling phenomena by introducing bandgap or splitting gap ($\delta = \omega_+ - \omega_-$) between the two coupled plasmon-phonon mode. For the experimental purpose, we apply PMMA via spin coating on the top of the FIB fabricated 2D-metasurface where the FTIR measurement and simulation shows a good agreement in the three individual cases.

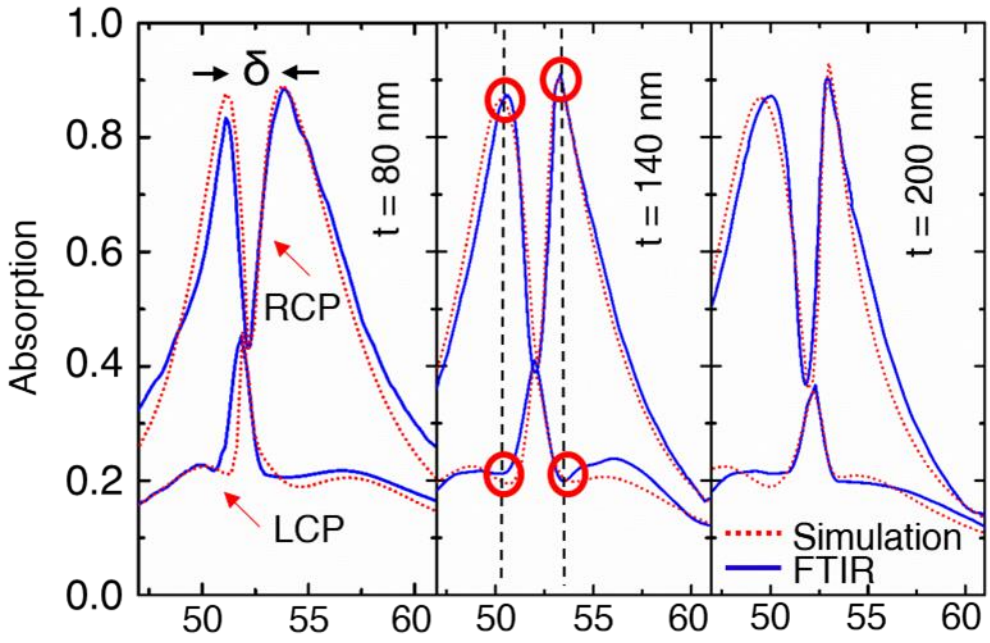

Figure 3.3 Spectra measurement in coupled condition while the thickness of the PMMA (t) is varied. The metasurface periodic condition is p*k1.

3.5. ANALYSIS OF THE SPLITTING BEHAVIOUR

We focus on the periodic structure of the metasurface to estimate the splitting behavior based on periodicity. Usually, in the coupling mode, the splitting gap increase with coupling strength [51-53]. In this regard, twenty-four samples in different periodic condition (p) are used to observe the coupling phenomena. The yellow dot line in the contour plot (Figure 3.5) shows the anticrossing behavior, and maximum coupling strength is in the frequency of 52 THz. When the p-value is small, the broad plasmon mode is far away from the molecular vibrational mode, and hence the interaction between these two modes results in a Fano-like resonance [54, 55].

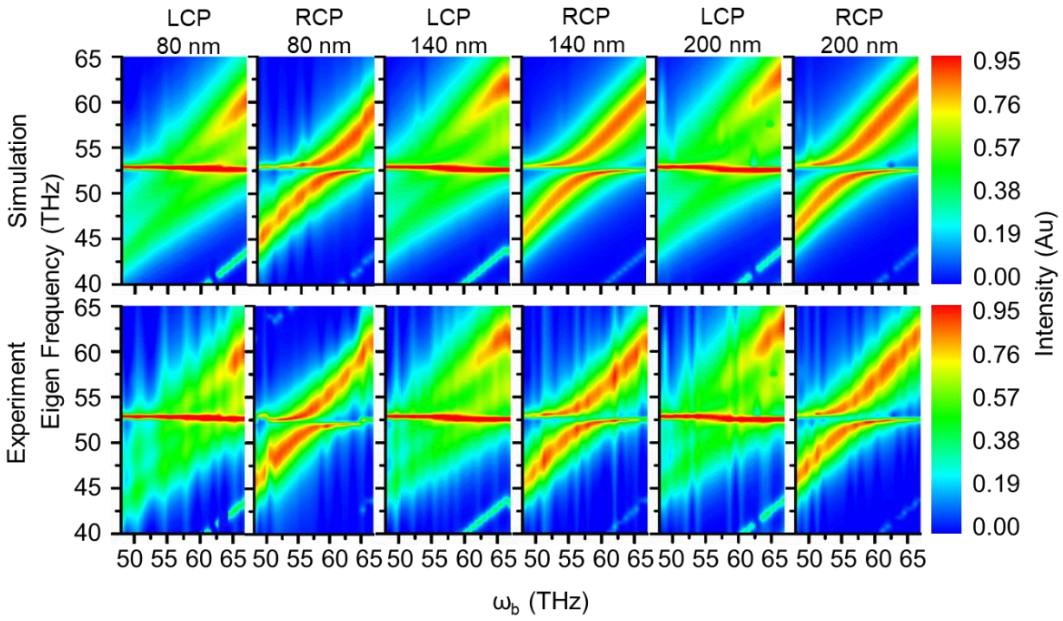

Figure 3.4 Bare metamaterials frequency as a function of coupled system frequency.

The broad plasmon mode change with the p-value where the smallest p-value shows the phonon vibration mode is far away from plasmon mode. But in resonance

condition two new hybrid modes is observed due to strong plasmon-phonon coupling. The coupling result also introduce the Rabi splitting behavior in the frequency of 52 THz. In our experiment, the full-width at half-maximum (FWHM) ($\zeta_{PLASMON}$) of the uncoupled plasmon resonance and molecular vibration (ζ_{PMMA}) satisfy the condition $\delta_{rabi} > (\zeta_{PMMA} + \zeta_{PLASMON})/2$, which is the criteria of Rabi splitting [41, 56, 57]. For Tunning, the anticrossing behavior, we take three different thicknesses (80 nm, 140 nm, 200 nm) of PMMA. Duel resonance features found in all the cases in both the numerical simulation and FTIR measurement. It is noticeable that the splitting gets higher with the increase of PMMA thickness. The most surprising thing observe that any particular PMMA thickness, the RCP splitting gap is much larger than the LCP splitting gap (δ). By changing PMMA thickness, we find the splitting gap (δ) in the case of RCP: 2.9 THz to 3.54 THz and for LCP: 2.44 THz to 3.02 THz. The RCP coupling strength is higher than the LCP coupling strength because the RCP electrometric field concentration is higher than the LCP. During the coupling condition, the energy loss in the RCP mode, some of the lost energy added in the LCP coupling. That is why the frequency where RCP absorption peaks go down in vice versa the LCP peaks go up seems like “M” and “W” (Figure 3.4). It is worth mentioning that our metasurface follows the dipole resonant mode, as is seen in Figure 3.5(a). The metasurface is designed intentionally in such a way that it could confine the electromagnetic field in the two-particular point of meta-structure, especially in the top and bottom surface of the inner elliptical structure. Figure 3.5(c) shows the electric field distribution in the Au-Al_2O_3-Au-PMMA medium in which the white dashed curved indicated in Figure 3.5(b). Hence, we calculate the optical power, which has overlapped between the PMMA molecules and resonance mode to

identify the strength of molecular interaction strength in the dipole resonant mode. The overlapped optical power described as:

$$p_{tot} = \int_0^z E_0 \exp(-2\sigma z)\, dz \propto A(1 - \exp(-2\sigma z)) + A_0 \quad (1)$$

Here A is a coefficient, σ is decay rate, and A_0 is the overlapped optical power. As overlapped optical power is proportional to splitting behavior so we can write the equation as,

$$\delta = A(1 - \exp(-2\sigma z)) + A_0 \quad (2)$$

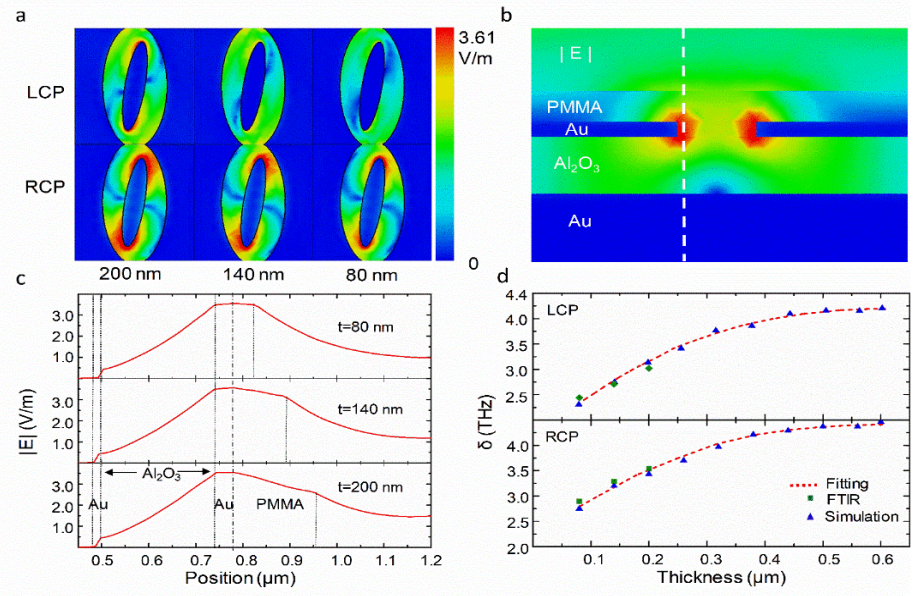

Figure 3.5 Electric field distribution across the metamaterial layers. (a) Top view of the Electromagnetic field in the plasmon-phonon coupling condition based on PMMA layer thickness (200, 140, and 80 nm). (b) The cross-section of the electric field distribution in the frequency of 52 THz. (c) The electric field profile in the multilayer structure based on PMMA layer thickness. The profile collection location (b) is pointed by the white dash line, and the incident wave is right circularly polarized light. (d) Comparison of splitting the gap between Fitting, FTIR, and simulated resulted as a function of PMMA layer thickness.

We simulated the PMMA thickness from 80-600 nm to figure out the overlapped optical power. The above equation (2) is fitted to find the parameters A, A_0, σ. The fitting result shows the value for the RCP: A= 2.85 THz, A_0=1.90 THz, σ=1.95 μm^{-1} and for LCP: A= 3.18 THz, A_0=1.48 THz, σ=1.77 μm^{-1}. Since the electrified in the plasmon-phonon coupling mode decay exponentially inside the PMMA layer so for variable thickness of the PMMA layer would have different overlapped with the confined plasmonic mode. Here the electric field confined in the metal surface, then it's gradually decaying in the surrounding medium (Figure 3.5) where the decay length (l_d) is approximately 350 nm for gold metasurface. The decay length is calculated as: $l_d = \frac{\lambda}{2\pi}\left(\frac{-n^4}{\varepsilon' + n^4}\right)^{-\frac{1}{2}}$. Inside that decay range l_d, with the increase of PMMA layer thickness, coupling strength increases. For the PMMA molecule above the range l_d, the forbidden energy gap becomes saturated because of weak plasmon phonon coupling (Figure 3.5(d)). It indicates that for LCP and RCP case, the overlap optical power is different, which can be tuned by varying the PMMA thickness.

4. CONCLUSION

In summary, we have successfully fabricated the 2D-chiral metasurface that has higher circular dichroism in the mid-infrared range. The experimental result shows that the polarization-dependent electromagnetic absorption leads to a high heat signature. That high heat signature with a strong chiroptical response helps to exhibit the thermal circular dichroism in the gold meta structure. It is also explainable that the meta structure resonance mode can be tuned either by changing the periodic structure or the curvature of the shape. Furthermore, multiple resonance structures with different sizes (n) broaden the absorption range in the midinfrared area, which has a significant application in broadband thermal emitter design. The experimental result shows the strong coupling phenomena between the PMMA molecules and the chiral metasurface, where this strong coupling presents the anticrossing behavior and satisfies the Rabi splitting. In the splitting, the RCP splitting gap is higher than the LCP splitting gap, which demonstrated that the circularly polarized light could be an effective parameter for molecules detection. Besides that, the strength of the coupling can be controlled by tuning the PMMA thickness, which represents the overlap optical power is proportional to the splitting gap of two plasmon-phonon eigenmodes. This splitting gap gradually increases until the end of decay length, and then it becomes saturated, which illustrates that the coupling strength is limited to a certain range of deposited molecules thickness. Therefore, the effect of circularly polarized light in broadband absorption, as well as molecules detection, will open further opportunities in thermal energy harvesting and chiral imaging.

BIBLIOGRAPHY

[1] F. Lu *et al.*, "Discrete nanocubes as plasmonic reporters of molecular chirality," *Nano letters,* vol. 13, no. 7, pp. 3145-3151, 2013.

[2] A. Ben-Moshe, B. M. Maoz, A. O. Govorov, and G. Markovich, "Chirality and chiroptical effects in inorganic nanocrystal systems with plasmon and exciton resonances," *Chemical Society Reviews,* vol. 42, no. 16, pp. 7028-7041, 2013.

[3] N. I. Landy, S. Sajuyigbe, J. J. Mock, D. R. Smith, and W. J. Padilla, "Perfect Metamaterial Absorber," *Physical Review Letters,* vol. 100, no. 20, p. 207402, 05/21/ 2008, doi: 10.1103/PhysRevLett.100.207402.

[4] Y. Cui *et al.*, "Plasmonic and metamaterial structures as electromagnetic absorbers," *Laser & Photonics Reviews,* vol. 8, no. 4, pp. 495-520, 2014, doi: 10.1002/lpor.201400026.

[5] H. Deng *et al.*, "Broadband perfect absorber based on one ultrathin layer of refractory metal," *Opt Lett,* vol. 40, no. 11, pp. 2592-5, Jun 1 2015, doi: 10.1364/OL.40.002592.

[6] E. Rephaeli and S. Fan, "Absorber and emitter for solar thermo-photovoltaic systems to achieve efficiency exceeding the Shockley-Queisser limit," *Opt Express,* vol. 17, no. 17, pp. 15145-59, Aug 17 2009, doi: 10.1364/oe.17.015145.

[7] H. A. Atwater and A. Polman, "Plasmonics for improved photovoltaic devices," *Nat Mater,* vol. 9, no. 3, pp. 205-13, Mar 2010, doi: 10.1038/nmat2629.

[8] C. Wu *et al.*, "Metamaterial-based integrated plasmonic absorber/emitter for solar thermo-photovoltaic systems," *Journal of Optics,* vol. 14, no. 2, p. 024005, 2012/01/12 2012, doi: 10.1088/2040-8978/14/2/024005.

[9] H. Deng, T. Wang, J. Gao, and X. Yang, "Metamaterial thermal emitters based on nanowire cavities for high-efficiency thermophotovoltaics," *Journal of Optics,* vol. 16, no. 3, p. 035102, 2014/02/04 2014, doi: 10.1088/2040-8978/16/3/035102.

[10] H. Wang, V. Prasad Sivan, A. Mitchell, G. Rosengarten, P. Phelan, and L. Wang, "Highly efficient selective metamaterial absorber for high-temperature solar thermal energy harvesting," *Solar Energy Materials and Solar Cells,* vol. 137, pp. 235-242, 2015/06/01/ 2015, doi: doi.org/10.1016/j.solmat.2015.02.019.

[11] D. Woolf, J. Hensley, J. G. Cederberg, D. T. Bethke, A. D. Grine, and E. A. Shaner, "Heterogeneous metasurface for high temperature selective emission," *Applied Physics Letters*, vol. 105, no. 8, p. 081110, 2014/08/25 2014, doi: 10.1063/1.4893742.

[12] D. Costantini *et al.*, "Plasmonic Metasurface for Directional and Frequency-Selective Thermal Emission," *Physical Review Applied*, vol. 4, no. 1, p. 014023, 07/30/ 2015, doi: 10.1103/PhysRevApplied.4.014023.

[13] C. Huang, X. Ma, M. Pu, G. Yi, Y. Wang, and X. Luo, "Dual-band 90° polarization rotator using twisted split ring resonators array," *Optics Communications*, vol. 291, pp. 345-348, 2013/03/15/ 2013, doi: doi.org/10.1016/j.optcom.2012.10.046.

[14] S. Zhang *et al.*, "Chiral Surface Plasmon Polaritons on Metallic Nanowires," *Physical Review Letters*, vol. 107, no. 9, p. 096801, 08/23/ 2011, doi: 10.1103/PhysRevLett.107.096801.

[15] M. Esposito *et al.*, "Nanoscale 3D Chiral Plasmonic Helices with Circular Dichroism at Visible Frequencies," *ACS Photonics*, vol. 2, no. 1, pp. 105-114, 2015/01/21 2015, doi: 10.1021/ph500318p.

[16] M. Esposito, V. Tasco, F. Todisco, A. Benedetti, D. Sanvitto, and A. Passaseo, "Three Dimensional Chiral Metamaterial Nanospirals in the Visible Range by Vertically Compensated Focused Ion Beam Induced-Deposition," *Advanced Optical Materials*, vol. 2, no. 2, pp. 154-161, 2014, doi: 10.1002/adom.201300323.

[17] J. K. Gansel *et al.*, "Gold Helix Photonic Metamaterial as Broadband Circular Polarizer," *Science*, vol. 325, no. 5947, pp. 1513-1515, 2009, doi: 10.1126/science.1177031.

[18] E. Togan *et al.*, "Quantum entanglement between an optical photon and a solid-state spin qubit," *Nature*, vol. 466, no. 7307, pp. 730-734, 2010/08/01 2010, doi: 10.1038/nature09256.

[19] H. S. Park, T.-T. Kim, H.-D. Kim, K. Kim, and B. Min, "Nondispersive optical activity of meshed helical metamaterials," *Nature Communications*, vol. 5, no. 1, p. 5435, 2014/11/17 2014, doi: 10.1038/ncomms6435.

[20] J. G. Fleming, S. Y. Lin, I. El-Kady, R. Biswas, and K. M. Ho, "All-metallic three-dimensional photonic crystals with a large infrared bandgap," *Nature*, vol. 417, no. 6884, pp. 52-55, 2002/05/01 2002, doi: 10.1038/417052a.

[21] L. P. Wang and Z. M. Zhang, "Phonon-mediated magnetic polaritons in the infrared region," *Optics Express,* vol. 19, no. S2, pp. A126-A135, 2011/03/14 2011, doi: 10.1364/OE.19.00A126.

[22] Z. Li, L. Stan, D. A. Czaplewski, X. Yang, and J. Gao, "Wavelength-selective mid-infrared metamaterial absorbers with multiple tungsten cross resonators," *Optics Express,* vol. 26, no. 5, pp. 5616-5631, 2018/03/05 2018, doi: 10.1364/OE.26.005616.

[23] Y. Chen, J. Gao, and X. Yang, "Chiral Metamaterials of Plasmonic Slanted Nanoapertures with Symmetry Breaking," *Nano Letters,* vol. 18, no. 1, pp. 520-527, 2018/01/10 2018, doi: 10.1021/acs.nanolett.7b04515.

[24] S. Wang, L. Kang, and D. H. Werner, "Active Terahertz Chiral Metamaterials Based on Phase Transition of Vanadium Dioxide (VO2)," *Scientific Reports,* vol. 8, no. 1, p. 189, 2018/01/09 2018, doi: 10.1038/s41598-017-18472-x.

[25] Y. Chen, X. Yang, and J. Gao, "Spin-controlled wavefront shaping with plasmonic chiral geometric metasurfaces," *Light: Science & Applications,* vol. 7, no. 1, p. 84, 2018/10/31 2018, doi: 10.1038/s41377-018-0086-x.

[26] A. D. Rakić, A. B. Djurišić, J. M. Elazar, and M. L. Majewski, "Optical properties of metallic films for vertical-cavity optoelectronic devices," *Appl. Opt.,* vol. 37, no. 22, pp. 5271-5283, 1998/08/01 1998, doi: 10.1364/AO.37.005271.

[27] J. Kischkat *et al.*, "Mid-infrared optical properties of thin films of aluminum oxide, titanium dioxide, silicon dioxide, aluminum nitride, and silicon nitride," *Appl. Opt.,* vol. 51, no. 28, pp. 6789-6798, 2012/10/01 2012, doi: 10.1364/AO.51.006789.

[28] K. A. Willets and R. P. V. Duyne, "Localized Surface Plasmon Resonance Spectroscopy and Sensing," *Annual Review of Physical Chemistry,* vol. 58, no. 1, pp. 267-297, 2007, doi: 10.1146/annurev.physchem.58.032806.104607.

[29] A. Hatef, S. M. Sadeghi, É. Boulais, and M. Meunier, "Quantum dot–metallic nanorod sensors via exciton–plasmon interaction," *Nanotechnology,* vol. 24, no. 1, p. 015502, 2012/12/05 2012, doi: 10.1088/0957-4484/24/1/015502.

[30] S. Zeng, D. Baillargeat, H.-P. Ho, and K.-T. Yong, "Nanomaterials enhanced surface plasmon resonance for biological and chemical sensing applications," *Chemical Society Reviews,* 10.1039/C3CS60479A vol. 43, no. 10, pp. 3426-3452, 2014, doi: 10.1039/C3CS60479A.

[31] T. Wang, V. H. Nguyen, A. Buchenauer, U. Schnakenberg, and T. Taubner, "Surface enhanced infrared spectroscopy with gold strip gratings," *Opt. Express,* vol. 21, no. 7, pp. 9005-9010, 2013/04/08 2013, doi: 10.1364/OE.21.009005.

[32] G. Dayal, X. Y. Chin, C. Soci, and R. Singh, "High-Q Plasmonic Fano Resonance for Multiband Surface-Enhanced Infrared Absorption of Molecular Vibrational Sensing," *Advanced Optical Materials,* vol. 5, no. 2, p. 1600559, 2017, doi: 10.1002/adom.201600559.

[33] R. A. Shelby, D. R. Smith, and S. Schultz, "Experimental verification of a negative index of refraction," *science,* vol. 292, no. 5514, pp. 77-79, 2001.

[34] N. Yu *et al.*, "Light propagation with phase discontinuities: generalized laws of reflection and refraction," *science,* vol. 334, no. 6054, pp. 333-337, 2011.

[35] M. Ren, E. Plum, J. Xu, and N. I. Zheludev, "Giant nonlinear optical activity in a plasmonic metamaterial," *Nature communications,* vol. 3, p. 833, 2012.

[36] S. P. Rodrigues *et al.*, "Intensity-dependent modulation of optically active signals in a chiral metamaterial," *Nature communications,* vol. 8, p. 14602, 2017.

[37] D. Schurig *et al.*, "Metamaterial electromagnetic cloak at microwave frequencies," *Science,* vol. 314, no. 5801, pp. 977-980, 2006.

[38] P. Georgi *et al.*, "Metasurface interferometry toward quantum sensors," *Light: Science & Applications,* vol. 8, no. 1, p. 70, 2019/08/14 2019, doi: 10.1038/s41377-019-0182-6.

[39] K. Ataka and J. Heberle, "Biochemical applications of surface-enhanced infrared absorption spectroscopy," (in eng), *Anal Bioanal Chem,* vol. 388, no. 1, pp. 47-54, 2007, doi: 10.1007/s00216-006-1071-4.

[40] A. Polyakov *et al.*, "Plasmon resonance tuning in metallic nanocavities," *Scientific Reports,* Article vol. 2, p. 933, 12/06/online 2012, doi: 10.1038/srep00933.

[41] P. Torma and W. L. Barnes, "Strong coupling between surface plasmon polaritons and emitters: a review," *Rep Prog Phys,* vol. 78, no. 1, p. 013901, Jan 2015, doi: 10.1088/0034-4885/78/1/013901.

[42] D. S. Dovzhenko, S. V. Ryabchuk, Y. P. Rakovich, and I. R. Nabiev, "Light-matter interaction in the strong coupling regime: configurations, conditions, and applications," *Nanoscale,* vol. 10, no. 8, pp. 3589-3605, Feb 22 2018, doi: 10.1039/c7nr06917k.

[43] A. Benz *et al.*, "Strong coupling in the sub-wavelength limit using metamaterial nanocavities," *Nat Commun,* vol. 4, p. 2882, 2013, doi: 10.1038/ncomms3882.

[44] S. Campione, A. Benz, J. F. Klem, M. B. Sinclair, I. Brener, and F. Capolino, "Electrodynamic modeling of strong coupling between a metasurface and intersubband transitions in quantum wells," *Physical Review B*, vol. 89, no. 16, p. 165133, 04/28/ 2014, doi: 10.1103/PhysRevB.89.165133.

[45] R. Adato *et al.*, "Ultra-sensitive vibrational spectroscopy of protein monolayers with plasmonic nanoantenna arrays," *Proceedings of the National Academy of Sciences*, vol. 106, no. 46, pp. 19227-19232, 2009, doi: 10.1073/pnas.0907459106.

[46] A. E. Cetin *et al.*, "Quantification of Multiple Molecular Fingerprints by Dual-Resonant Perfect Absorber," *Advanced Optical Materials*, vol. 4, no. 8, pp. 1274-1280, 2016/08/01 2016, doi: 10.1002/adom.201600305.

[47] D.-H. Kwon, P. L. Werner, and D. H. Werner, "Optical planar chiral metamaterial designs for strong circular dichroism and polarization rotation," *Opt. Express*, vol. 16, no. 16, pp. 11802-11807, 2008/08/04 2008, doi: 10.1364/OE.16.011802.

[48] W. Wan, X. Yang, and J. Gao, "Strong coupling between mid-infrared localized plasmons and phonons," *Opt. Express*, vol. 24, no. 11, pp. 12367-12374, 2016/05/30 2016, doi: 10.1364/OE.24.012367.

[49] B. Tang, Z. Li, E. Palacios, Z. Liu, S. Butun, and K. Aydin, "Chiral-Selective Plasmonic Metasurface Absorbers Operating at Visible Frequencies," *IEEE Photonics Technology Letters*, vol. 29, no. 3, pp. 295-298, 2017, doi: 10.1109/LPT.2016.2647262.

[50] Y. Lee, S.-J. Kim, H. Park, and B. Lee, "Metamaterials and Metasurfaces for Sensor Applications," (in eng), *Sensors (Basel)*, vol. 17, no. 8, p. 1726, 2017, doi: 10.3390/s17081726.

[51] D. J. Shelton *et al.*, "Strong Coupling between Nanoscale Metamaterials and Phonons," *Nano Letters*, vol. 11, no. 5, pp. 2104-2108, 2011/05/11 2011, doi: 10.1021/nl200689z.

[52] X. Zhang, D. Wu, C. Sun, and X. Zhang, "Artificial phonon-plasmon polariton at the interface of piezoelectric metamaterials and semiconductors," *Physical Review B*, vol. 76, p. 85318, 08/01 2007, doi: 10.1103/PhysRevB.76.085318.

[53] B. Lahiri, S. G. McMeekin, R. M. De La Rue, and N. P. Johnson, "Enhanced Fano resonance of organic material films deposited on arrays of asymmetric split-ring resonators (A-SRRs)," *Opt. Express*, vol. 21, no. 8, pp. 9343-9352, 2013/04/22 2013, doi: 10.1364/OE.21.009343.

[54] N. T. Fofang, T.-H. Park, O. Neumann, N. A. Mirin, P. Nordlander, and N. J. Halas, "Plexcitonic nanoparticles: plasmon− exciton coupling in nanoshell− J-aggregate complexes," *Nano letters,* vol. 8, no. 10, pp. 3481-3487, 2008.

[55] S. Savasta, R. Saija, A. Ridolfo, O. Di Stefano, P. Denti, and F. Borghese, "Nanopolaritons: vacuum Rabi splitting with a single quantum dot in the center of a dimer nanoantenna," *ACS nano,* vol. 4, no. 11, pp. 6369-6376, 2010.

[56] X. Liu *et al.*, "Strong light–matter coupling in two-dimensional atomic crystals," *Nature Photonics,* vol. 9, no. 1, p. 30, 2015.

[57] E.-M. Roller, C. Argyropoulos, A. Högele, T. Liedl, and M. Pilo-Pais, "Plasmon–exciton coupling using DNA templates," *Nano letters,* vol. 16, no. 9, pp. 5962-5966, 2016.

VITA

Md Shamim Mahmud was born in Khulna, Bangladesh. He received his Bachelor of Science degree in Naval Architecture and Marine Engineering from Bangladesh University of Engineering and Technology in February 2013. He earned his Master of Engineering degree from Texas State University in July 2018. After that he wanted to pursue another graduate degree and came to Missouri University of Science and Technology in Rolla, Missouri, USA in August 2018. He started working as a Graduate Research Assistant in August 2018. He received his Master of Science degree in Mechanical Engineering from Missouri University of Science and Technology in December 2020.